Published in final edited form as:
Aerosol Sci Technol. 2014 July 1; 47(7): 768–776. doi:10.1080/02786826.2014.925536.

Physicochemical Characterization of Simulated Welding Fume from a Spark Discharge System

Jae Hong Park[1], **Imali A. Mudunkotuwa**[2], **Jong Sung Kim**[3,4], **Aditya Stanam**[4], **Peter S. Thorne**[1,4], **Vicki H. Grassian**[2,4], and **Thomas M. Peters**[1,4,*]

[1]Department of Occupational and Environmental Health, University of Iowa, Iowa, USA

[2]Department of Chemistry, University of Iowa, Iowa, USA

[3]Department of Community Health and Epidemiology, Dalhousie University, Halifax, NS, Canada

[4]Interdisciplinary Graduate Program in Human Toxicology, University of Iowa, Iowa, USA

Abstract

This study introduces spark discharge system (SDS) as a way to simulate welding fumes. The SDS was developed using welding rods as electrodes with an optional coagulation chamber. The size, morphology, composition, and concentration of the fume produced and the concentration of ozone (O_3) and nitrogen oxides (NO_X) were characterized. The number median diameter (NMD) and total number concentration (TNC) of fresh fume particles were ranged 10–23 nm and 3.1×10^7–6×10^7 particles/cm^3, respectively. For fresh fume particles, the total mass concentration (TMC) measured gravimetrically ranged 85–760 μg/m^3. The size distribution was stable over a period of 12 h. The NMD and TNC of aged fume particles were ranged 81–154 nm and 1.5×10^6–2.7×10^6 particles/cm^3, respectively. The composition of the aged fume particles was dominated by Fe and O with an estimated stoichiometry between that of Fe_2O_3 and Fe_3O_4. Concentrations of O_3 and NO_X were ranged 0.07–2.2 ppm and 1–20 ppm, respectively. These results indicate that the SDS is capable of producing stable fumes over a long-period that are similar to actual welding fumes. This system may be useful in toxicological studies and evaluation of instrumentation.

1. INTRODUCTION

Welding produces “welding fume” which is mixture of metal oxide particles (Jenkins and Eagar 2005) and gases including ozone (O_3) and nitrogen oxides (NO_X) (Antonini 2003). Welding vaporizes metals found in the object being welded and materials used in the welding process (e.g., welding sticks used in shielded metal arc welding, SMAW). These metals react with ambient air, condense, and form metal oxide particles primarily of respirable size (Antonini 2003). In welding, O_3 is produced in a photochemical reaction induced by ultraviolet light with ambient oxygen gas during the welding process (Liu et al. 2007), and NO_X are formed by direct oxidation of ambient nitrogen (N_2) at high temperatures produced by the arc or flame (Antonini 2003).

Address correspondence to Thomas M. Peters, 105 River St, S331 CPHB, University of Iowa, Iowa City, IA 52242, USA. Thomas-m-peters@uiowa.edu.

Welding fume particles range in size from 0.005 to 20 μm, although less than 10–30% of the fume mass is larger than 1 μm (Jenkins and Eagar 2005). When inhaled, sub-micrometer particles can deposit throughout the respiratory system. As a result of their small size and unique properties *in vivo*, the toxicological profiles of sub-micrometer particles, including nanoparticles, may differ considerably from those of larger particles composed of the same materials (Oberdörster et al. 1992). It has been established that adverse pulmonary health effects are primarily dependent on the size, solubility and chemical makeup of the particle (Oprya el al. 2012; Kim et al. 2011a). The welding fume particles that deposit in the respiratory tract can dissolve and/or translocate as nanoparticles from the lung, reach the bloodstream, and pass to other organs (Antonini et al., 2009; Antonini et al., 2010). The materials that are welded often contain alloying elements, such as manganese (Mn) common to all steel, chromium (Cr) in stainless steel, and cadmium (Cd) in plating and brazing materials. These metals contribute to the toxicity of welding fume and can cause acute and chronic adverse health effects (Antonini 2003).

O_3 and NO_X are potent oxidizing agents that can also contribute to adverse health effects. Prolonged exposure to low levels of O_3 (as low as 0.08 ppm) can initiate pulmonary inflammatory reactions in normal humans (Devlin et al. 1991), potentiate allergic airway diseases (Holz et al. 2002). Repeated exposures to low levels (i.e. 0.2 ppm) of O_3 led to persistent airway inflammation in healthy subjects (Jörres et al. 2000). Exposure to low level ozone (i.e. 0.06 ppm for 6.6 hours) induced a significant decrease in lung function (i.e. forced expiratory volume in one second, FEV1) with inflammatory changes in the airways of healthy young adults (Kim et al. 2011b). Repeated low level (i.e. 2 ppm) exposure to nitrogen dioxide (NO_2) induced pro-allergic responses (i.e. upregulation of IL-5, IL-10, IL-13, and ICAM-1 expression) in the bronchial epithelium of healthy human airways (Pathmanathan et al. 2003). Brief exposure to environmentally relevant concentration (i.e. 0.27 ppm) of NO_2 can enhance the airway inflammatory reaction to allergen without any decrement in lung function in asthmatics (Barck et al. 2005). Prolonged exposure to low doses (i.e. 0.5 ppm) of nitric oxide (NO) induced interstitial lung damage in rats (Mercer et al. 1995).

The ability to control welding fume concentrations is critical in toxicological studies. Only few welding fume inhalation exposure systems have been developed because of the numerous different types of welding processes employed in the workplace and the difficulties with generating a fume with stable output over extended periods of time. Hicks et al. (1984) used experienced welders to generate fumes from various welding types for the head-only exposure and the intratracheal instillation. Difficulties with this system included the need to hire experienced welders to operate the system and disruptions in output because the base metal and welding materials required replacement every few minutes. Others have developed robotic welders to generate fumes. Oh et al. (2012) used a rotating stainless disc as a base metal and a welding rod restrained in the welding rod holder support to simulate SMAW fume, known informally as stick welding. Similarly, Zimmer et al. (2002) used a welding fume generation system comprised of a rotating cylinder as the base material. Antonini et al. (2006; 2007) developed a robotic welding fume generator to simulate gas metal arc welding (GMAW). The welding fume generation system used an automated,

programmable six-axis robotic arm, a water-cooled arc welding torch, a wire feeder that supplied the wire to the torch, and an automatic welding torch cleaner to keep the welding nozzle free of debris and spatter. This system was coupled with an inhalation exposure system. Physical and chemical characterizations of the generated fumes were performed. Although quite representative of real welding exposures, a limitation of these robotic systems is their large size, high cost, and complex operation that introduce difficulties in performing laboratory experiments.

On the other hand, spark systems represent a simple way to reproducibly generate a metal oxide aerosol of controllable size and concentration (Roth et al. 2004). A spark is discharged across the electrode gap when a high voltage is supplied to metal electrodes, thereby vaporizing material from the electrodes and producing primary particles in the low nanometer size range via nucleation/condensation of the vapor. At the same time, these particles are oxidized by air ions and radicals produced by spark discharge. Primary particles collide with one another, due to a relative motion between them and adhere to form chain-like agglomerates (Meuller et al. 2012). This spark process is similar to SMAW. Many researchers have discussed and described the application of spark discharge in conductive nanoparticle (metals and carbon) generation for toxicology study (Roth et al. 2004; Kapp et al. 2004; Takenaka et al. 2006; Messing et al. 2013). However, none of these studies sought to simulate welding fume.

The focus of this study was twofold. First, we introduce a spark discharge system (SDS) as a way to simulate welding fume in a compact system that is inexpensive and easy to control. The SDS was developed using welding rods as electrodes with an optional chamber that can then be used to coagulate the particles. Second, the physicochemical characteristics of particles and gases produced by the SDS were characterized. In particular, for particles, the size, morphology, aggregation state and composition of the welding fumes produced under an air environment were determined using a variety of analytical methods. This novel application of SDS can be used to simulate welding fume from SMAW for toxicological studies and instrument testing.

2. METHODS

2.1. Spark Discharge System

The SDS is shown in Figure 1. Compressed air was passed through a trap to remove oil contaminants, a diffusion dryer to remove moisture, and a high efficiency particulate air (HEPA) filter to remove particles. The dry, clean air, controlled by a needle valve and monitored with a mass flowmeter (4146, TSI Inc., USA), was delivered at 5 L/min to the spark discharge chamber (volume 10.6 cm^3). In the chamber, a spark discharge was formed between two identical electrodes. The electrodes were coaxial welding rods (Hard Surfacing Stick Electrodes Overlay; Hobart, USA) with a core rod (diameter 3.2 mm = 1/8 in.) and a coating layer (diameter 6.4 mm = 1/4 in.). Elemental and compositional specifications of these electrodes are provided in Table 1. The electrical circuit included a resistance of 0.5 MΩ (two 1 MΩ resistors arranged in parallel), a capacitance of 1 nF, and an applied voltage of 5 kV.

The aerosol produced by the spark was passed through an aerosol neutralizer (3087, TSI Inc., USA) to neutralize the charge on the aerosol to a Boltzmann distribution. Optionally, particles were delivered to a coagulation chamber, consisting of a circular steel cylinder with a volume of 0.18 m^3 (inner diameter of 0.39 m and length of 1.5 m). A coagulation time of 36 min was approximated from the volume of the coagulation chamber (0.180 m^3) divided by airflow rate (5 L/min).

2.2. Particle Size and Morphology

The aerosol produced by the SDS was characterized for the following conditions: without passing through the coagulation chamber (fresh fume) with loading currents of 0.25 mA, 0.5 mA, and 1 mA; and with passing through the coagulation chamber (aged fume) with loading currents of 1 mA and 3 mA. When the loading current increases, the generation rate and size of particles are also increased (Meuller et al. 2012). To identify operational conditions showing similar output to actual welding fumes, the loading currents were varied from 0.25 to 3 mA. The loading current was decreased from 1 to 0.25 mA to produce smaller sized particles for the fresh fume, and increased from 1 to 3 mA to produce lager sized particles for the aged fume. The spark and coagulation chambers were cleaned periodically with compressed dry particle-free air to eliminate the residual particles.

The size distributions of the generated particles were measured using a scanning mobility particle sizer (SMPS; 3936, TSI Inc., USA), consisting of a classifier controller (3080, TSI Inc., USA), a differential mobility analyzer (DMA), a condensation particle counter (CPC; 3776, TSI Inc., USA), and an aerosol neutralizer (3077; TSI Inc., USA). The SMPS was operated with a nano DMA (3085, TSI Inc., USA) to measure the fresh fume particles from 2.2 to 63.8 nm (mobility equivalent diameters) and a long DMA to measure the aged fume particles from 15.1 to 661.2 nm. The size distribution of each test atmosphere was measured five times. The size distributions of fresh fume particles were measured every 30 min for 12 h at loading currents of 0.25 mA and 0.5 mA to examine the long-term stability of generation.

To determine the total mass concentration, fresh and aged fume particles were sampled onto a polyvinyl chloride (PVC) membrane filter (5 μm, 37 mm, SKC Gulf Coast Inc., USA) at the sampling flow rate of 4 L/min for 12 h. A micro-balance (MT5, Mettler-Toledo, USA) was used to measure the weight of deposited particles. Gravimetric tests were conducted in triplicate.

To examine morphology, fresh and aged fume particles were sampled onto a transmission electron microscope (TEM) grid (200-mesh, Ni grid, Carbon layer, 01840N-F, Ted Pella Inc., USA). The TEM grid was placed on the PVC filter. Fresh fume particles (0.25 mA) and aged fume particles (3 mA) were sampled for 6 h and 5 min, respectively. A TEM (JEM-1230, JEOL Ltd, Japan) was used to evaluate the projected area diameter (d_{PA}) and morphology of generated particles. The d_{PA} is defined as the diameter of the circle having the same projected area as the particle's two-dimensional silhouette. The projected area (PA) was obtained using ImageJ software (version 1.47, NIH, USA) and d_{PA} was calculated as follows:

$$d_{PA}=2\times\sqrt{\frac{PA}{\pi}} \quad (1)$$

A total number of 100 and 70 agglomerates were counted for fresh and aged fume particles, respectively.

2.3. Chemical Characterization

Elemental analysis of aged fume particles was determined using energy dispersive X-ray (EDX) spectroscopy. To obtain EDX spectra, the fume particles deposited on the 200-mesh, carbon coated Ni grid were imaged by high resolution transmission electron microscopy (HRTEM) using a microscope (JEM-2100F, JEOL Ltd, Japan) in dark field mode. The EDX spectral peaks were compared against the standard peak positions of the elements given in Table 1. The elemental maps were obtained by rastering the electron beam over a specified region on the Ni grid. Mapping was conducted only for the aged fume particles because the loading of fresh fume particles collected on the grids was too low.

To further examine the phase of particles, aged fume particles with a loading current of 3 mA were collected onto a PVC filter for 36 hours. Insufficient mass of particles were collected for lower loading currents. The solid phase of the particles were determined by X-ray diffraction (XRD; Miniflex II, Rigaku Corporation, Japan) using Co K_α radiation (λ = 179 pm) at a step size of 0.02°. Cobalt is used as the source of X-rays to minimize the background resulting from iron fluorescence. The XRD patterns obtained were matched against a database containing standard patterns using the JADE software (version 8, Materials Data, Inc. USA) to identify the phases present in these particles.

2.4. O_3 and NO_X Generation

A gas monitor (PortaSensII, ATI, USA) was used to monitor O_3 and NO_X concentrations when the SDS was operating. The sensitivity of the instrument was 0.01 ppm for O_3 and 1 ppm for NO_X. Gas concentrations were measured in triplicate for each test condition.

3. RESULTS AND DISCUSSION

3.1. Particle Size and Morphology

The size distribution of the fresh and aged fume particles obtained by SMPS is shown in Figure 2 with summary details provided in Table 2. Images showing the morphology and size of the generated welding fume particles are shown in Figure 3. These data demonstrate that higher current supplied to the welding rod produces higher number concentrations and larger nanoparticles.

3.1.1. Fresh Fume Particles—For fresh fume particles, the number median diameter (NMD) increased from 10 nm at 0.25 mA to 23 nm at 1 mA. Similarly, the total number concentration (TNC) increased from 3.1×10^7 particles/cm^3 at 0.25 mA to 6×10^7 particles/cm^3 at 1 mA. Size distributions of fresh fume particles were log-normally distributed with a geometric standard deviation (σ_g) ranging from 1.52 to 1.64. As shown in

Figure 2c, the concentration and size distribution of the fresh fume particles were extremely stable over 12 h. The coefficient of variation of the 30-min readings over the 12-h period were: 2.9% TNC, 2.7% NMD, and 1.0% σ_g at a loading current of 0.25 mA; and 1.7% TNC, 2.7% NMD, and 0.5% σ_g at a loading current of 0.5 mA.

As shown in Figure 3a, fresh fume particles appeared as clusters and chain-like aggregates formed from much smaller primary particles sized 2.7 (±0.7) nm. A histogram of the primary particle diameter determined from analysis of TEM images is shown in Figure 3d. However, these primary particles appeared as imperfect spheres. Roth et al. (2004) explained that the primary particles in the spark discharge process form by nucleation and grow further either by collision with product molecules (condensation) or particles (coagulation). The colliding particles maintain their identity or fuse together into a single particle. This fusion can be complete or incomplete. In the case of iron oxide particles, incomplete fusion (partial sintering) occurred, and thus iron oxide particles appear as non-spherical particles. From TEM images, the mean d_{PA} of the fresh fume particles at 0.25 mA was 14 (±8.1) nm, which is consistent although somewhat larger than NMD (10 nm) from the SMPS (Table 2). However, the standard deviation of d_{PA} was ±8.1 nm and the difference of NMD and mean d_{PA} was within the range of error.

As shown in Table 2, the total mass concentrations (TMC) measured by SMPS did not agree well with that measured gravimetrically. The TMC measured by SMPS was 282 μg/m^3 at 0.25 mA and 7200 μg/m^3 at 1 mA, whereas the TMC measured gravimetrically was 85 μg/m^3 at 0.25 mA and 760 μg/m^3 at 1 mA. The TMC from SMPS was calculated from the measured number concentration assuming a particle density of 7870 kg/m^3 (bulk iron density) and spherical shape. The particles were observed to be highly non-spherical. Thus, the assumption of sphericity is problematical and the actual particle density is likely substantially lower than that of bulk iron.

These results show that the SDS when operated without the coagulation chamber can be used to generate fresh fume particles which consist primarily of nanoparticles in the range of 3 to 20 nm over a long time period. A major advantage of this method is that freshly produced nanoparticles can be immediately delivered to animals or cells without intermediary steps, such as nebulized suspension of powders. Generally, nanoparticles can be generated by dispersion of solutions or suspensions by nebulizers or electrospray, but the impurities of the dispersed liquid will contaminate the particles (Roth et al. 2004). Although nanoparticle production using vaporization of material in a tube furnace with subsequent homogenous nucleation, condensation, and coagulation offers similar benefits, the tube furnace system is considerably more complex and costly than the SDS used here. Additionally, impurities that evaporate from crucibles and tube materials are incorporated in the particles generated with a tube furnace system (Roth et al. 1994). Another advantage of SDS is that size and generation rate of fresh fume particles can be readily controlled by a loading current.

3.1.2. Aged Fume Particles—As expected when the fresh fume was passed through the coagulation chamber at a loading current of 1.0 mA, the NMD increased from 23 nm to 81 nm, and the TNC decreased from 6.0×10^7 to 1.5×10^6 particles/cm^3 (Figure 2b; Table 2).

When the current was increased to 3 mA, the NMD increased to 154 nm and the TNC increased to 2.7×10^6 particles/cm^3. Size distributions of aged fume particles were log-normally distributed but the σ_g was approximately 2, which was substantially larger than that for the fresh fume particles.

The size distribution of the aged fume particles observed at 3 mA is similar to that of a field study analyzing welding fume particles (Zimmer 2002; Stephenson et al. 2003). Using TEM, Zimmer (2002) identified the particles formed during welding to range in size from 50 to 300 nm. Stephenson et al. (2003) reported that welding produced an approximately lognormal particle mode with a 120-nm count median and a σ_g of 2.07.

Similar to fresh fume particles (Figure 3a), aged fume particles also appear as clusters and chain-like aggregates formed from much smaller primary particles (Figure 3b). The shape of aged fume particles is similar to one of welding fume sampled by Stephenson et al. (2003) and Antonini et al. (2006). The mean d_{PA} of the aged particles was 153 (±118.3) nm which agrees well with the NMD of 154 nm in Table 2. These aged fume particles can be used to evaluate instruments for welding fumes. Conventional methods to produce test aerosol have used salt, oil, and polystyrene sphere particles. Their shapes are cubes or spheres which are different from those of welding fumes. The SDS can be an alternative method to evaluate the instruments which measure the welding fumes.

As shown in Table 2, the TMC measured gravimetrically (730 μg/m^3 at 1 mA and 2700 μg/m^3 at 3 mA) were substantially lower than those from the SMPS (4.5×10^4 μg/m^3 at 1 mA and 2.4×10^5 μg/m^3 at 3 mA) (Table 2). The difference of TMC from SMPS and the gravimetric method for aged fume particles was substantially greater than that for fresh fume particles. A possible reason is the shape of the aged fume that the difference of particle density and assumed density was increased. The shape of aged fume particles was totally different with sphere and more complex than one of fresh fume particles as shown in Figure 3b. We may expect that the density of aged fume particle is smaller than 150 kg/m^3 from the result of gravimetric method.

The maximum TMC of 2700 μg/m^3 is comparable to eight-hour average concentrations measured in actual factories (3000 to 11300 μg/m^3, Balkhyour and Goknil, 2010). However, in toxicology studies, the required test concentration is often higher than 2700 μg/m^3. In traditional methods, welding fumes have been generated at concentrations near or above the recommended welding fume threshold exposure limit value-time weighted average (TLV-TWA) of 5000 μg/m^3 for 8 h/day (ACGIH, 2001). Antonini et al. (2006; 2007) have proposed welding fume concentrations of 1000–40000 μg/m^3 and 15000–40000 μg/m^3, respectively. These higher values of concentration can be easily realized by increasing the power input with increasing the loading current or the applied voltage (Meuller et al. 2012).

3.2. Chemical Characteristics

The EDX elemental analysis of collected particles generated under coagulated conditions at 3 mA is shown in Figure 4a. The peak at approximately 7.5 keV corresponds to the Ni grid used to support the sample and is not from the aged fume particles. The composition of the aged fume particles was similar to that of test electrodes and dominated by Fe and O. The

fractions of Fe and O were 0.08 and 0.15, respectively. From this result, a projected stoichiometry of iron oxide is between Fe_2O_3 and Fe_3O_4.

The first image in Figure 4b is for aged fume particles at 3 mA. The image of these particles is combined with EDX maps. These maps correspond to Fe, O, Si, Cr, and Ni, respectively. The dots in these images indicate the positions of each element in the first image. For example, Fe and O are concentrated in the regions corresponding to the particles in the first image, which shows that the particles contain Fe and O in agreement with spectrum shown in Figure 4a.

The powder XRD pattern (Figure 5) indicates that there are crystalline as well as amorphous materials present in the sample. In particular, the XRD data indicates that the crystalline fraction of spark-generated particles consists mainly of Fe_2O_3 (hematite) and Fe_3O_4 (magnetite), consistent with the EDX analysis. Sampled particles were reddish brown in color as shown in the inset of Figure 5 and have similar appearance to the laboratory synthesized 2 nm α-Fe_2O_3 nanoparticles. The broad band observed in the XRD patterns without any background subtraction indicates the presence of amorphous regions as well in these samples. In addition, majority of the background noise in the XRD patterns result from the fluorescence of iron and some from the X-rays scattered from air and the sample holder.

3.3. O_3 and NO_X Generation

The concentrations of O_3 and NO_X produced when the SDS was operating are provided in Table 3. A higher loading current resulted in higher concentrations of O_3 and NO_X. O_3 and NO_X emission was proportional to the loading current. The O_3 and NO_X concentrations increased from 0.07 and 1 ppm at 0.25 mA to 2.22 and 20 ppm at 3 mA.

Although other researchers have described the application of spark discharge for toxicology study (Roth et al. 2004; Kapp et al. 2004; Takenaka et al. 2006; Messing et al. 2013), they have not focused on gases since they used spark discharge with inert gas such as argon or N_2. Our results of using spark discharge in an air environment show that O_3 and NO_X are produced, like that typical of SMAW in an occupational setting. However, we are unable to control the O_3 and NO_X emissions. In some toxicological studies, particles and gases need to be separated. In future work we will investigate the use of inert gas, such as N_2, for the spark environment with mixing of oxygen after particles are formed to minimize O_3 and NO_X production.

These gas concentrations are similar to those observed during welding on worksites. Steel (1968) measured concentration of O_3 in the range of 0.1 to 0.6 ppm in 40 shipyards where three different welding processes were used. Liu et al. (2007) observed that O_3 concentrations were highest (~0.20 ppm) for SMAW and gradually decreased to 0.06 ppm 10 min after the welding was completed. NO_2 levels in the welding area can be as high as 7 ppm during flux-cored arc welding (Antonini, 2003). Cole et al. (2007) conducted GMAW and gas tungsten arc welding processes for various combinations of base and filler alloys to quantify gas emissions such as O_3, NO, and NO_2. O_3 concentration was ranged from 0.37 to 4.70 ppm. NO and NO_2 concentrations were 0.52–16.6 ppm and 0.24–7.85 ppm, respectively.

4. CONCLUSION

This study introduces a method of particle generation using spark discharge to simulate welding fume. The SDS was developed using welding rods as electrodes with an optional chamber that can be used to coagulate the particles. Operating the spark under an air environment, we characterized the size, morphology, concentration, and composition of the welding fume particles and concentrations of O_3 and NO_X. These results indicate that the generated fume is comparable to welding fume particles in workplace settings. Our SDS may be useful in toxicological studies and instrument testing. The SDS as described here is limited to SMAW. A further limitation of this study is that only one welding rod was tested. Future studies will focus on particle generation in inert gas environments to eliminate these gases using various types of welding rod used in SMAW.

Acknowledgments

This work was supported by a pilot research grant from the Environmental Health Sciences Research Center at the University of Iowa (NIH P30 ES005605). Financial support was also provided by National Institute for Occupational Safety and Health (1 R01 OH010238).

References

ACGIH. Welding fumes, not otherwise specified; Documentation of the Threshold Limit values for Chemical Substances, Vol. 3. American Conference of Governmental Industrial Hygienists; Cincinnati, OH: ACGIH; 2001. p. 1726-1727.

Antonini J. Health Effects of Welding. Crit Rev Toxicol. 2003; 33(1):61–103. [PubMed: 12585507]

Antonini JM, Afshari AA, Stone S, Chen B, Schwegler-Berry D, Fletcher WG, Goldsmith WT, Vandestouwe KH, McKinney W, Castranova V, Frazer DG. Design, Construction, and Characterization of a Novel Robotic Welding Fume Generator and Inhalation Exposure System for Laboratory Animals. J Occup Envrion Hyg. 2006; 3(4):194–203.

Antonini JM, Stone S, Roberts JR, Chen B, Schwegler-Berry D, Afshari AA, Frazer DG. Effect of Short-Term Stainless Steel Welding Fume Inhalation Exposure on Lung Inflammation, Injury, and Defense Responses in Rats. Toxicol Appl Pharm. 2007; 223(3):234–245.

Antonini JM, Sriram K, Benkovic SA, Roberts JR, Stone S, Chen BT, Schwegler-Berry D, Jefferson AM, Billig BK, Felton CM, Hammer MA, Ma F, Frazer DG, O'Callaghan JP, Miller DB. Mild steel welding fume causes manganese accumulation and subtle neuroinflammatory changes but not overt neuronal damage in discrete brain regions of rats after short-term inhalation exposure. Neurotoxicology. 2009; 30(6):915–925. [PubMed: 19782702]

Antonini JM, Roberts JR, Chapman RS, Soukup JM, Ghio AJ, Sriram K. Pulmonary toxicity and extrapulmonary tissue distribution of metals after repeated exposure to different welding fumes. Inhal Toxicol. 2010; 22(10):805–816. [PubMed: 20560776]

Balkhyour MA, Goknil MK. Total fume and metal concentrations during welding in selected factories in Jeddah, Saudi Arabia. Int J Environ Res Publ Health. 2010; 7(7):2978–2987.

Barck C, Lundahl J, Halldén G, Bylin G. Brief Exposures to NO_2 Augment the Allergic Inflammation in Asthmatics. Environ Res. 2005; 97(1):58–66. [PubMed: 15476734]

Cole H, Epstein S, Peace J. Particulate and Gaseous Emissions When Welding Aluminum Alloys. J Occup Environ Hyg. 2007; 4(9):678–687. [PubMed: 17620189]

Devlin RB, McDonnell WF, Mann R, Becker S, House DE, Schreinemachers D, Koren HS. Exposure of Humans to Ambient Levels of Ozone for 6.6 Hours Causes Cellular and Biochemical Changes in the Lung. Am J Resp Cell Mol. 1991; 4(1):72–81.

Hicks R, Lam HF, Al-Shamma KJ, Hewitt PJ. Pneumoconiotic Effects of Welding-Fume Particles from Mild and Stainless Steel Deposited in the Lung of the Rat. Arch Toxicol. 1984; 55(1):1–10. [PubMed: 6732500]

Hobart. Material Safety Data Sheet #230. Selectrode Industries, Inc; 2008.

Holz O, Mucke M, Paasch K, Bohme S, Timm P, Richter K, Magnussen H, Jörres RA. Repeated Ozone Exposures Enhance Bronchial Allergen Responses in Subjects with Rhinitis or Asthma. Clin Exp Allergy. 2002; 32(5):681–689. [PubMed: 11994090]

Jenkins NT, Eagar TW. Chemical Analysis of Welding Fume Particles. Weld J. 2005; 84(6):87s–93s.

Jörres RA, Holz O, Zachgo W, Timm P, Koschyk S, Muller B, Grimminger F, Seeger W, Kelly FJ, Dunster C, Frischer T, Lubec G, Waschewski M, Niendorf A, Magnussen H. The Effect of Repeated Ozone Exposures on Inflammatory Markers in Bronchoalveolar Lavage Fluid and Mucosal Biopsies. Am J Resp Crit Care. 2000; 161(6):1855–1861.

Kapp N, Kreyling W, Schulz H, Im Hof V, Gehr P, Semmler M, Geiser M. Electron Energy Loss Spectroscopy for Analysis of Inhaled Ultrafine Particles in Rat Lungs. Microsc Res Techiq. 2004; 63(5):298–305.

Kim JS, Adamčaková-Dodd A, O'Shaughnessy PT, Grassian VH, Thorne PS. Effects of Copper Nanoparticle Exposure on Host Defense in a Murine Pulmonary Infection Model. Part Fibre Toxicol. 2011a; 8(1):29. [PubMed: 21943386]

Kim CS, Alexis NE, Rappold AG, Kehrl H, Hazucha MJ, Lay JC, Schmitt MT, Case M, Devlin RB, Peden DB, Diaz-Sanchez D. Lung Function and Inflammatory Responses in Healthy Young Adults Exposed to 0.06 ppm Ozone for 6.6 Hours. Am J Resp Crit Care. 2011b; 183(9):1215–1221.

Liu HH, Wu YC, Chen HL. Production of Ozone and Reactive Oxygen Species After Welding. Arch Environ Con Tox. 2007; 53(4):513–518.

Mercer RR, Costa DL, Crapo JD. Effects of Prolonged Exposure to Low Doses of Nitric Oxide or Nitrogen Dioxide on the Alveolar Septa of the Adult Rat Lung. Lab Invest. 1995; 73(1):20–28. [PubMed: 7603036]

Messing ME, Svensson CR, Pagels J, Meuller BO, Deppert K, Rissler J. Gas-Borne Particles with Tunable and Highly Controlled Characteristics for Nanotoxicology Studies. Nanotoxicology. 2013; 7(6):1052–1063. [PubMed: 22630037]

Meuller BO, Messing ME, Engberg DL, Jansson AM, Johansson LI, Norlén SM, Tureson N, Deppert K. Review of Spark Discharge Generators for Production of Nanoparticle Aerosols. Aerosol Sci Technol. 2012; 46(11):1256–1270.

Oberdörster G, Ferin J, Gelein R, Soderholm SC, Finkelstein J. Role of the Alveolar Macrophage in Lung Injury: Studies with Ultrafine Particles. Environ Health Persp. 1992; 97:193–199.

Oh JH, Yang MJ, Heo JD, Yang YS, Park HJ, Park SM, Kwon MS, Song CW, Yoon S, Yu IJ. Inflammatory Response in Rat Lungs with Recurrent Exposure to Welding Fumes a Tanscriptomic Approach. Toxicol Ind Health. 2012; 28(3):203–215. [PubMed: 21730038]

Oprya M, Kiro S, Worobiec A, Horemans B, Darchuk L, Novakovic V, Ennan A, Van Grieken R. Size Distribution and Chemical Properties of Welding Fumes of Inhalable Particles. J Aerosol Sci. 2012; 45:50–57.

Pathmanathan S, Krishna MT, Blomberg A, Helleday R, Kelly FJ, Sandström T, Holgate ST, Wilson SJ, Frew AJ. Repeated Daily Exposure to 2 ppm Nitrogen Dioxide Upregulates the Expression of IL-5, IL-10, IL-13, and ICAM-1 in the Bronchial Epithelium of Healthy Human Airways. Occup Environ Med. 2003; 60(11):892–896. [PubMed: 14573722]

Roth C, Scheuch G, Stahlhofen W. Clearance Measurements with Radioactively Labelled Ultrafine Particles. Ann Occup Hyg. 1994; 38:101–106. inhaled particles VII.

Roth C, Ferron GA, Karg E, Lentner B, Schumann G, Takenaka S, Heyder J. Generation of Ultrafine Particles by Spark Discharge. Aerosol Sci Technol. 2004; 38(3):228–235.

Steel J. Respiratory Hazards in Shipbuilding and Shiprepairing. Ann Occup Hyg. 1968; 11(2):115–121. [PubMed: 5654324]

Stephenson D, Seshadri G, Veranth JM. Workplace Exposure to Submicron Particle Mass and Number Concentrations from Manual Arc Welding of Carbon Steel. AIHA J. 2003; 64(4):516–521.

Takenaka S, Karg E, Kreyling WG, Lentner B, Möller W, Behnke-Semmler M, Jennen L, Walch A, Michalke B, Schramel P, Heyder J, Schulz H. Distribution Pattern of Inhaled Ultrafine Gold Particles in the Rat Lung. Inhal Toxicol. 2006; 18(10):733–740. [PubMed: 16774862]

Zimmer AT, Baron PA, Biswas P. The Influence of Operating Parameters on Number-Weighted Aerosol Size Distribution Generated from a Gas Metal Arc Welding Process. J Aerosol Sci. 2002; 33(3):519–531.

Zimmer AT. The Influence of Metallurgy on the Formation of Welding Aerosols. J Environ Monitor. 2002; 4 (5):628–632.

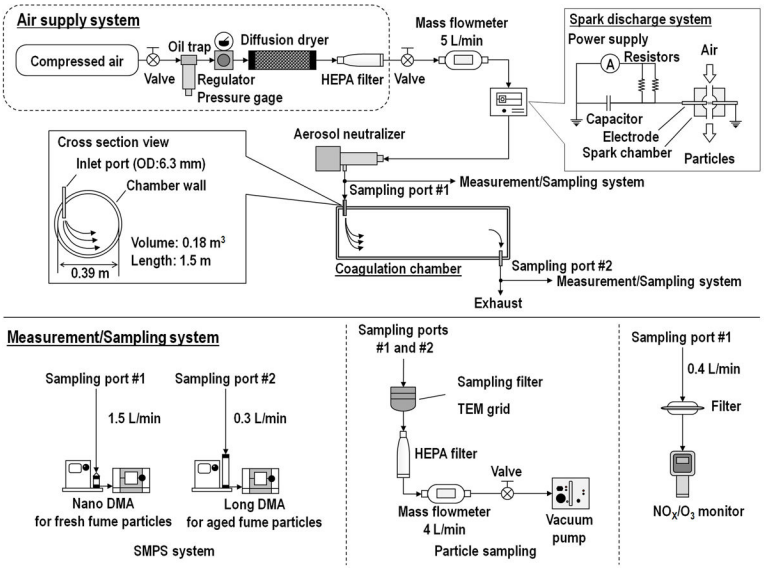

FIG. 1.

Experimental setup. Sampling ports #1 and #2 are located before and after the coagulation chamber, respectively.

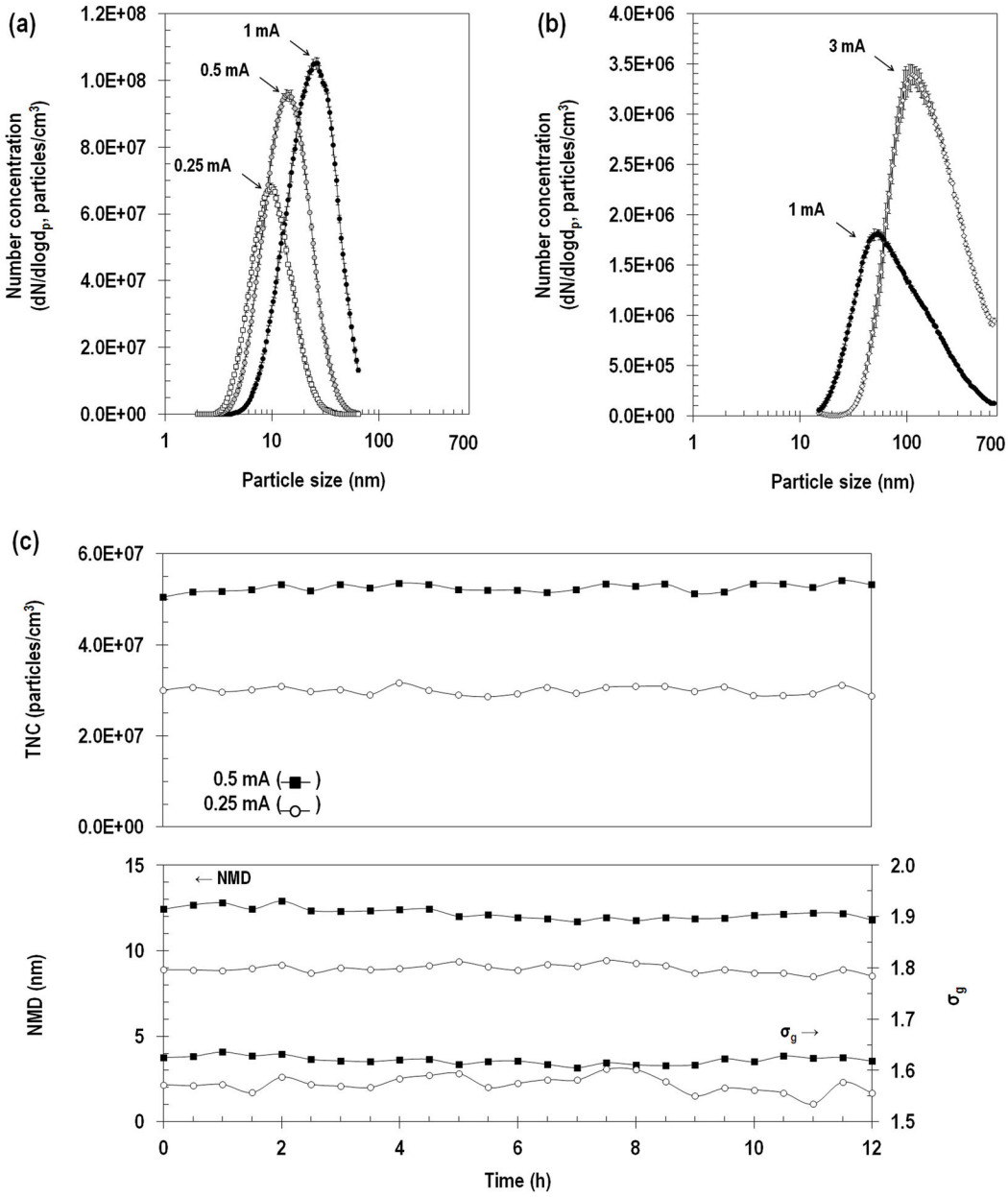

FIG. 2.

Size distributions of fresh (a) and aged (b) fume particles and continuous generation data (c) of fresh fume particles at 0.25 and 0.5 mA. TNC: Total number concentration; NMD: number median diameter; σ_g: geometric standard deviation.

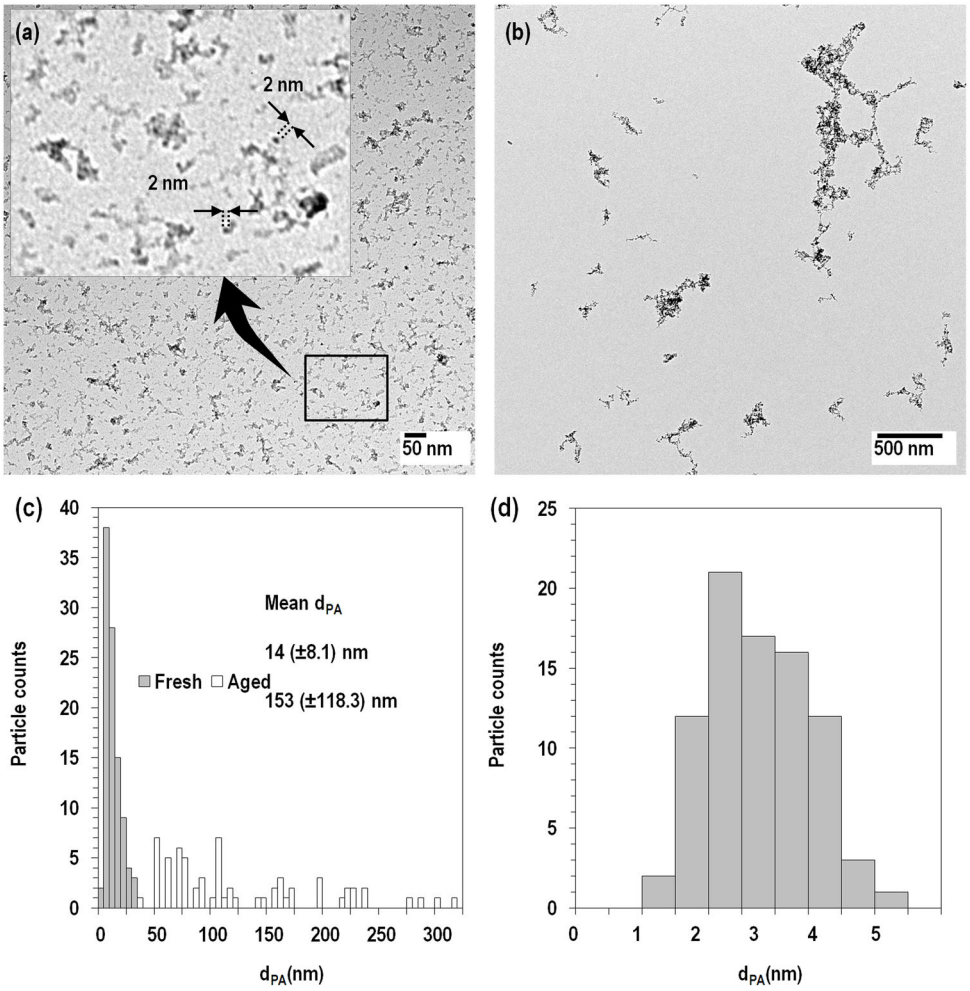

FIG. 3.

TEM images of fresh (a) and aged (b) fume particles, projected area diameters (d_{PA}) of fresh and aged fume particles (c) and primary single particles (d).

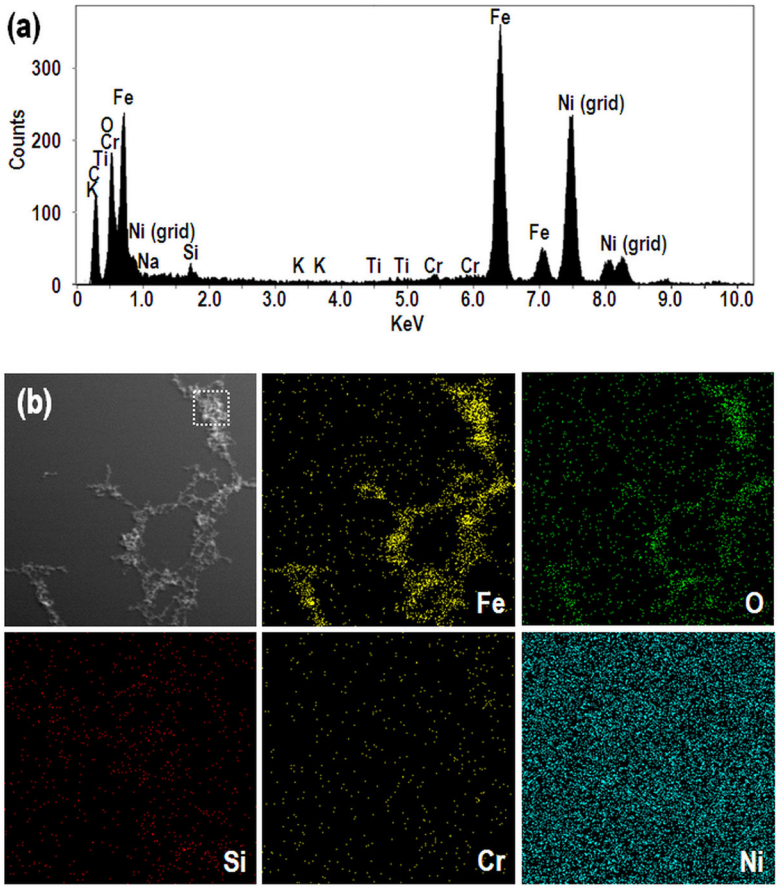

FIG. 4.

EDX spectrum (a) and elemental maps (b) of aged fume particles. These maps are for Fe, O, Si, Cr and Ni. For EDX spectrum, the square region in the top left image of Figure 5b was analyzed. Particles were sampled on the Ni grid.

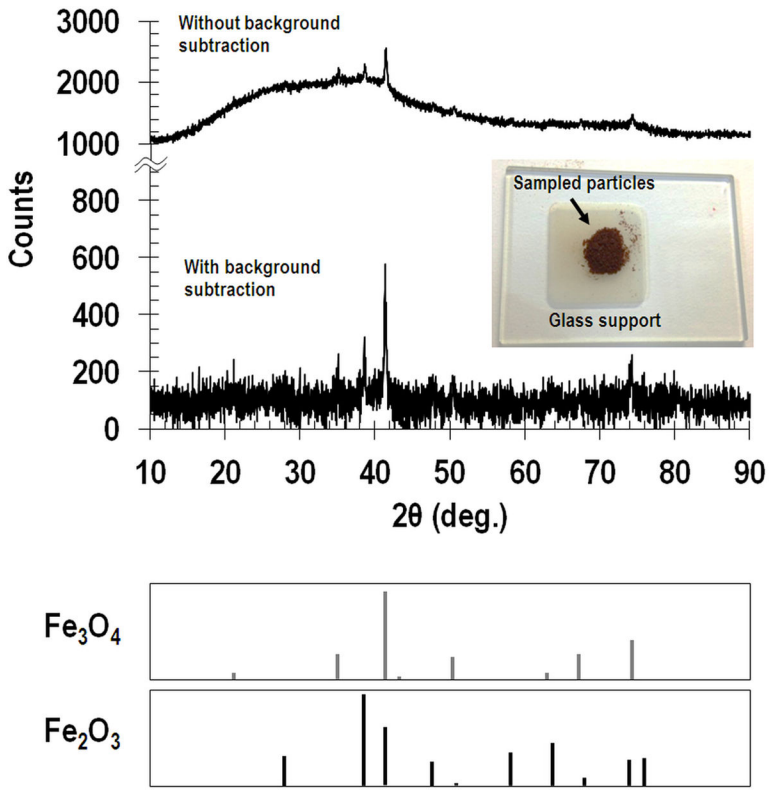

FIG. 5.

XRD pattern of aged fume particles and basic patterns of Fe_3O_4 and Fe_2O_3.

Table 1

Elemental and compositional specification of test electrodes (Hobart, 2008)

Element	Core rod	Coating layer
Fe	Balance	60–70%
C	< 0.15%	0.1–2.1%
Si	< 0.7%	0.1–2.1%
Mn	< 1.0%	0.1–2.0%
V	-	0.1–2.1%
Cr	-	5–15%
Mo	-	1–11%
TiO_2	-	1–11%
W	-	1–11%
Calcium Carbonate ($CaCO_3$)	-	1–11%
Chromium Fluoride (CrF_3)	-	1–11%
Sodium Silicate (Na_2O_3Si)	-	1–11%
Potassium Silicate (K_2O_3Si)	-	1–11%

Table 2

Sample current and particle characteristics (size, total number concentration and total mass concentration) for generated welding fume particles

	Loading current (mA)	NMD (nm)	σ_g	Total number concentration (particles/cm^3)	Total mass concentration (μg/m^3)	
					SMPS	Gravimetric
Fresh fume particles	0.25	10 (±0.1)	1.52 (±0.01)	3.1×10^7 ($\pm6.6\times10^5$)	282 (±26)	85 (±4)
	0.5	14 (±0.2)	1.59 (±0.01)	5.1×10^7 ($\pm2.5\times10^5$)	1418 (±108)	220 (±5)
	1	23 (±0.1)	1.64 (±0.01)	6.0×10^7 ($\pm8.9\times10^5$)	7196 (±172)	760 (±70)
Aged fume particles	1	81 (±1.1)	2.16 (±0.01)	1.5×10^6 ($\pm1.8\times10^4$)	4.5×10^4 ($\pm4.0\times10^2$)	730 (±40)
	3	154 (±3.0)	1.95 (±0.02)	2.7×10^6 ($\pm7.0\times10^4$)	2.4×10^5 ($\pm2.9\times10^3$)	2700 (±550)

(*Note* NMD: Number median diameter, σ_g: geometric standard deviation. Particle density was assumed as 7870 kg/m^3 (bulk iron density) for the SMPS.)

Table 3

O_3 and NO_X concentrations measured for spark discharge system under different operating conditions

Loading current (mA)	O_3 (ppm)	NO_X (ppm)
0.25	0.07 (±0.01)	1 (±0)
0.5	0.26 (±0.01)	3 (±0)
1	0.62 (±0.01)	7 (±1)
3	2.22 (±0.01)	20 (±1)